Research Square

Preprints are preliminary reports that have not undergone peer review.
They should not be considered conclusive, used to inform clinical practice,
or referenced by the media as validated information.

Time-like Ribbon Frames and Magnetic Curves in Minkowski 3-Space: Killing Fields, Cyclotron Motion and Spin Precession

MUSTAFA YENEROĞLU

myeneroglu@firat.edu.tr

Fırat University

Research Article

Keywords: Minkowski space, Ribbon frame, Magnetic curve, Killing magnetic field, Thomas–BMT spin precession, Relativistic cyclotron motion

Posted Date: November 18th, 2026

DOI: https://doi.org/10.21203/rs.3.rs-11645603/v1

License: This work is licensed under a Creative Commons Attribution 4.0 International License.
Read Full License

Additional Declarations: No competing interests reported.

Time-like Ribbon Frames and Magnetic Curves in Minkowski 3-Space: Killing Fields, Cyclotron Motion and Spin Precession

Abstract

Moving frames along curves turn the Lorentz force of a magnetic field into a short list of scalar equations, and in Minkowski space they also describe charged particles moving close to the speed of light. A ribbon frame suited to curves with inflection points has been proposed for time-like curves, but its equations were copied from the Euclidean case and do not preserve the Lorentzian metric. We derive the time-like ribbon frame from the Lorentzian cross product, characterize the three families of frame-adapted magnetic curves by necessary and sufficient conditions, and prove that the Darboux field is the only field that transports the whole frame. For Killing magnetic fields we obtain a closed scalar system with two first integrals, and we show that the curvature is fixed by position through a conserved charge. Numerical integrations confirm every identity to within about one part in a hundred billion, and they show that a radial electric field drives a trajectory to infinity in finite proper time with the predicted rate. Reading curvature and torsion as rest-frame electric and magnetic fields gives relativistic cyclotron and hyperbolic motion. Adding a spin vector yields a one-line angle equation that reproduces Thomas precession, the anomalous precession frequency of storage-ring experiments, the magic muon momentum of 3.094 GeV/c and the proton value of 0.7007 GeV/c. The framework therefore links the geometry of curves with spin dynamics in particle accelerators and gives a frame that stays well defined where Frenet methods fail.

Keywords Minkowski space · Ribbon frame · Magnetic curve · Killing magnetic field · Thomas–BMT spin precession · Relativistic cyclotron motion

Mathematics Subject Classification 53B30 · 53A35 · 53C50 · 78A35 · 83A05

Significance Statement

Fast charged particles trace curves in spacetime. We describe them with a moving frame that survives points of zero curvature and correct a sign error inherited from Euclidean formulas. One angle equation then recovers Thomas precession and the magic momenta of muon and proton storage rings.

1 Introduction

A magnetic curve is a curve $\boldsymbol{\gamma}$ that satisfies $\nabla_{\boldsymbol{\gamma}'}\boldsymbol{\gamma}' = \boldsymbol{\Phi}(\boldsymbol{\gamma}')$, where $\boldsymbol{\Phi}$ is the Lorentz force of a closed 2-form; in dimension three the 2-form is encoded by a divergence-free vector field $\boldsymbol{V}$. Barros and Romero linked magnetic trajectories with vortex filaments and elastic rods [1]. Bozkurt and co-authors gave a frame-based treatment in Riemannian 3-manifolds [2], and Özdemir and co-authors extended it to semi-Riemannian manifolds, where causal characters enter the equations [3]. A recent survey collects these developments and lists open questions on frames and causal structure [4].

Killing magnetic fields are both physically natural and mathematically tractable, because their flow preserves the metric. Druţă-Romaniuc and Munteanu classified Killing magnetic curves in Minkowski 3-space $\mathbb{E}_1^3$ [5], Munteanu and Nistor solved the problem in $\mathbb{S}^2 \times \mathbb{R}$ [6], and Jiang and Pei treated lightlike magnetic

curves in $\mathbb{E}_1^3$ [7]. Inoguchi and Munteanu analyzed the stability of magnetic trajectories through magnetic Jacobi fields [8]. These works rely on Frenet frames, which require non-vanishing curvature, and so leave open what happens at inflection points.

Frames without this restriction come from computational geometry and molecular biology. Bishop introduced the parallel frame [9], Farouki reviewed its rational versions [10], and Özdemir and Ergin constructed parallel frames for non-lightlike curves in $\mathbb{E}_1^3$ [11]. Bohr and Markvorsen introduced the ribbon frame for ribbon crystals, motivated by DNA and polymers [12, 13]. In this journal, Altınkaya built magnetic curves on a conjugate rotation-minimizing frame [14], and Öztürk and Öztürk studied non-helical loxodromes in the Heisenberg group [15]. Körpınar, Demirkol and co-authors applied Frenet-type and Bishop frames to magnetic and flux-surface problems [16-19]. Ribbon-frame magnetic curves in $\mathbb{E}_1^3$ were first considered in a recent thesis [20], in which the Euclidean ribbon equations were transferred without change. The resulting frame is not orthonormal for the Lorentzian metric, and the resulting force matrices are not the Lorentz force of any field.

A second gap concerns physics. A time-like unit-speed curve is the worldline of an observer, its curvature is the proper acceleration, and the Lorentz law is a magnetic-curve equation [21-23]. Thomas showed that a gyroscope on an accelerated worldline precesses [24], and Bargmann, Michel and Telegdi (BMT) wrote the covariant spin equation [25]. The BMT equation underlies the muon $g-2$ measurements at CERN and Brookhaven [26, 27] and at Fermilab [28-30], the planned J-PARC experiment [31], and storage-ring searches for electric dipole moments [32-35]. Refs. [5, 7, 14] treat magnetic curves without spin, while Refs. [21, 25] treat spin without a frame adapted to the curve.

This paper closes both gaps for time-like curves. First, we derive the time-like ribbon frame with Lorentzian signs and identify the Fermi–Walker frame as its Bishop-type companion. Second, we characterize $\boldsymbol{e}$-, $\boldsymbol{f}$- and $\boldsymbol{g}$-magnetic curves and prove that the Darboux vector is the unique field transporting the whole frame. Third, for Killing fields we obtain a closed scalar system with two first integrals, show that the curvature is fixed by position, and compute the escape time in a radial electric field. Fourth, we read curvature and torsion as rest-frame electric and magnetic fields. Fifth, we write the spin equation in the ribbon frame and obtain an angle law that recovers Thomas precession, the spin tune and the magic momenta of storage rings. Sections 2–4 develop the geometry, Sections 5–7 the electromagnetic reading, Killing and uniform fields, and Section 8 the spin. Section 9 compares with the literature, and Section 10 concludes.

2 Lorentzian preliminaries

The Minkowski space $\mathbb{E}_1^3$ is $\mathbb{R}^3$ with the coordinates (x, y, t) and the metric $\langle \boldsymbol{u}, \boldsymbol{v} \rangle = u_1 v_1 + u_2 v_2 - u_3 v_3$. A vector $\boldsymbol{v}$ is space-like if $\langle \boldsymbol{v}, \boldsymbol{v} \rangle > 0$ or $\boldsymbol{v} = \boldsymbol{0}$, time-like if $\langle \boldsymbol{v}, \boldsymbol{v} \rangle < 0$, and null if $\langle \boldsymbol{v}, \boldsymbol{v} \rangle = 0$ and $\boldsymbol{v} \neq \boldsymbol{0}$. We use units with $c = 1$ throughout. The Lorentzian cross product is

$$\boldsymbol{u} \wedge \boldsymbol{v} = (u_3 v_2 - u_2 v_3,\ u_1 v_3 - u_3 v_1,\ u_1 v_2 - u_2 v_1),$$

and it satisfies

$$\langle \boldsymbol{u} \wedge \boldsymbol{v}, \boldsymbol{w} \rangle = -\det(\boldsymbol{u}, \boldsymbol{v}, \boldsymbol{w}). \tag{1}$$

Identity (1) shows that $\boldsymbol{u}\wedge\boldsymbol{v}$ is orthogonal to $\boldsymbol{u}$ and $\boldsymbol{v}$ and that the map $\boldsymbol{X}\mapsto\boldsymbol{V}\wedge\boldsymbol{X}$ is skew-adjoint for every fixed $\boldsymbol{V}$.

Lemma 1. Let $\{\boldsymbol{e},\boldsymbol{f},\boldsymbol{g}\}$ be an orthonormal frame with $\boldsymbol{e}$ time-like, $\boldsymbol{f},\boldsymbol{g}$ space-like and $\boldsymbol{e}\wedge\boldsymbol{f}=\boldsymbol{g}$. Then

(2)

$$\boldsymbol{e}\wedge\boldsymbol{f}=\boldsymbol{g},\qquad \boldsymbol{f}\wedge\boldsymbol{g}=-\boldsymbol{e},\qquad \boldsymbol{g}\wedge\boldsymbol{e}=\boldsymbol{f}.$$

Proof. By (1), $1=\langle\boldsymbol{g},\boldsymbol{g}\rangle=\langle\boldsymbol{e}\wedge\boldsymbol{f},\boldsymbol{g}\rangle=-\det(\boldsymbol{e},\boldsymbol{f},\boldsymbol{g})$, so $\det(\boldsymbol{e},\boldsymbol{f},\boldsymbol{g})=-1$. Then $\langle\boldsymbol{f}\wedge\boldsymbol{g},\boldsymbol{e}\rangle=-\det(\boldsymbol{f},\boldsymbol{g},\boldsymbol{e})=1$, and $\boldsymbol{f}\wedge\boldsymbol{g}$ is orthogonal to $\boldsymbol{f}$ and $\boldsymbol{g}$. Hence $\boldsymbol{f}\wedge\boldsymbol{g}=\langle\boldsymbol{f}\wedge\boldsymbol{g},\boldsymbol{e}\rangle\,\boldsymbol{e}/\langle\boldsymbol{e},\boldsymbol{e}\rangle=-\boldsymbol{e}$. Likewise $\langle\boldsymbol{g}\wedge\boldsymbol{e},\boldsymbol{f}\rangle=1$, and $\boldsymbol{g}\wedge\boldsymbol{e}$ is orthogonal to $\boldsymbol{e}$ and $\boldsymbol{g}$, which gives $\boldsymbol{g}\wedge\boldsymbol{e}=\boldsymbol{f}$. □

Relations (2) differ from the Euclidean rule $\boldsymbol{f}\times\boldsymbol{g}=\boldsymbol{e}$ by one sign. Using the Euclidean rule in $\mathbb{E}^3_1$ is the source of every error corrected in this paper.

A unit-speed time-like curve $\boldsymbol{\gamma}$ satisfies $\langle\boldsymbol{\gamma}',\boldsymbol{\gamma}'\rangle=-1$, so its parameter s is proper time. Where the curvature is non-zero it has a Frenet frame $\{\boldsymbol{t},\boldsymbol{n},\boldsymbol{t}\wedge\boldsymbol{n}\}$ with $\boldsymbol{t}=\boldsymbol{\gamma}'$, and [36]

(3)

$$\boldsymbol{t}'=\kappa\boldsymbol{n},\qquad \boldsymbol{n}'=\kappa\boldsymbol{t}+\tau\,\boldsymbol{t}\wedge\boldsymbol{n},\qquad (\boldsymbol{t}\wedge\boldsymbol{n})'=-\tau\boldsymbol{n},$$

with curvature $\kappa>0$ and torsion $\tau:=\langle\boldsymbol{n}',\boldsymbol{t}\wedge\boldsymbol{n}\rangle$. Physically, κ is the magnitude of the proper acceleration. A ribbon frame $\{\boldsymbol{e},\boldsymbol{f},\boldsymbol{g}\}$ of $\boldsymbol{\gamma}$ has $\boldsymbol{e}=\boldsymbol{\gamma}'$ and satisfies [12]

(4)

$$\boldsymbol{X}'=\boldsymbol{D}\wedge\boldsymbol{X},\qquad \boldsymbol{X}\in\{\boldsymbol{e},\boldsymbol{f},\boldsymbol{g}\},\qquad \boldsymbol{D}=\omega\boldsymbol{A},$$

where $\boldsymbol{A}$ is a unit vector field in $\operatorname{span}\{\boldsymbol{e},\boldsymbol{g}\}$ and $\omega\neq0$. The vector $\boldsymbol{D}$ is the Darboux vector of the frame. Where the curvature is non-zero, $\boldsymbol{f}=\pm\boldsymbol{n}$ and $\boldsymbol{g}=\pm\boldsymbol{t}\wedge\boldsymbol{n}$.

The Fermi–Walker derivative transports vectors along an accelerated worldline without rotation [23]. For a field $\boldsymbol{X}$ along $\boldsymbol{\gamma}$ with $\langle\boldsymbol{X},\boldsymbol{e}\rangle=0$ it reads

(5)

$$\frac{D_{\mathrm{FW}}\boldsymbol{X}}{ds}=\boldsymbol{X}'-\langle\boldsymbol{X},\boldsymbol{e}'\rangle\,\boldsymbol{e}.$$

A vector with vanishing Fermi–Walker derivative models the axis of a gyroscope carried by the observer. Table 1 lists the symbols used in the paper.

Table 1 Nomenclature. All quantities are dimensionless in units with $c=1$ and charge-to-mass ratio $q/m=1$

Symbol	Meaning	Symbol	Meaning
$\langle\cdot,\cdot\rangle$, $\wedge$	Lorentzian metric and cross product of $\mathbb{E}^3_1$	B, $\boldsymbol{E}$	rest-frame magnetic (pseudo-scalar) and electric fields, Eq. (19)
$\boldsymbol{\gamma}(s)$, s	unit-speed time-like curve (worldline) and its proper time	$\boldsymbol{K}=\boldsymbol{u}+\boldsymbol{w}\wedge\boldsymbol{p}$	Killing field with constants $\boldsymbol{u},\boldsymbol{w}$; w_1,w_2,w_3 frame components of $\boldsymbol{w}$
$\{\boldsymbol{e},\boldsymbol{f},\boldsymbol{g}\}$	ribbon frame, $\boldsymbol{e}=\boldsymbol{\gamma}'$ time-like, $\boldsymbol{g}=\boldsymbol{e}\wedge\boldsymbol{f}$	ϖ	invariant field strength $\sqrt{\lvert\langle\boldsymbol{D},\boldsymbol{D}\rangle\rvert}$ for uniform fields
a, b	signed ribbon curvature and ribbon torsion, Eq. (6)	γ_{L}, v	laboratory Lorentz factor and speed
κ, τ	Frenet curvature ($\kappa=\lvert a\rvert$) and torsion ($\lvert\tau\rvert=\lvert b\rvert$)	$\boldsymbol{S}$, φ	spin vector and its angle from $\boldsymbol{f}$ towards $\boldsymbol{g}$
$\boldsymbol{D}$, ω, θ	Darboux vector, its magnitude and its hyperbolic angle with $\boldsymbol{g}$	g, a	gyromagnetic factor and anomaly $\mathsf{a}=g/2-1$
$\boldsymbol{V}$, $\boldsymbol{\Phi}$	field vector and Lorentz force $\boldsymbol{\Phi}(\boldsymbol{X})=$	χ, ν	electric share of the centripetal force

Symbol	Meaning	Symbol	Meaning
	$\boldsymbol{V} \wedge \boldsymbol{X}$		and spin tune
$\Omega, \lambda, \Omega_2$	free functions of $\boldsymbol{e}$-, $\boldsymbol{f}$- and $\boldsymbol{g}$-magnetic curves	$\gamma_{\mathrm{m}}, p_{\mathrm{m}}$	magic Lorentz factor and magic momentum

3 The time-like ribbon frame

We now derive the ribbon frame with the Lorentzian relations. Let $\boldsymbol{e}$ be time-like, let $\boldsymbol{f}, \boldsymbol{g}$ be space-like with $\boldsymbol{e} \wedge \boldsymbol{f} = \boldsymbol{g}$, and let θ be the hyperbolic angle between $\boldsymbol{g}$ and $\boldsymbol{D}$. Two cases occur, depending on the causal character of the Darboux vector.

Proposition 1. (a) If $\boldsymbol{D}$ is space-like, then $\boldsymbol{A} = \sinh\theta\, \boldsymbol{e} - \cosh\theta\, \boldsymbol{g}$. (b) If $\boldsymbol{D}$ is time-like, then $\boldsymbol{A} = \cosh\theta\, \boldsymbol{e} + \sinh\theta\, \boldsymbol{g}$. In both cases

(6)

$$\boldsymbol{e}' = a\, \boldsymbol{f}, \qquad \boldsymbol{f}' = a\, \boldsymbol{e} + b\, \boldsymbol{g}, \qquad \boldsymbol{g}' = -b\, \boldsymbol{f},$$

with $(a, b) = (-\omega\cosh\theta,\ \omega\sinh\theta)$ in case (a) and $(a, b) = (\omega\sinh\theta,\ \omega\cosh\theta)$ in case (b), and

(7)

$$\boldsymbol{D} = b\, \boldsymbol{e} + a\, \boldsymbol{g}, \qquad \langle \boldsymbol{D}, \boldsymbol{D} \rangle = a^2 - b^2.$$

Proof. (a) By (2), $\boldsymbol{A} \wedge \boldsymbol{e} = -\cosh\theta\, \boldsymbol{f}$. Since $\boldsymbol{g} \wedge \boldsymbol{f} = \boldsymbol{e}$, we have $\boldsymbol{A} \wedge \boldsymbol{f} = \sinh\theta\, \boldsymbol{g} - \cosh\theta\, \boldsymbol{e}$, and $\boldsymbol{A} \wedge \boldsymbol{g} = -\sinh\theta\, \boldsymbol{f}$. Multiplying by ω and using (4) gives (6). (b) Similarly $\boldsymbol{A} \wedge \boldsymbol{e} = \sinh\theta\, \boldsymbol{f}$, $\boldsymbol{A} \wedge \boldsymbol{f} = \cosh\theta\, \boldsymbol{g} + \sinh\theta\, \boldsymbol{e}$ and $\boldsymbol{A} \wedge \boldsymbol{g} = -\cosh\theta\, \boldsymbol{f}$. Finally $\omega \boldsymbol{A} = b\, \boldsymbol{e} + a\, \boldsymbol{g}$ in both cases, and $\langle \boldsymbol{D}, \boldsymbol{D} \rangle = -b^2 + a^2$. □

Lemma 2. System (6) preserves orthonormality, because $\langle \boldsymbol{e}', \boldsymbol{f} \rangle + \langle \boldsymbol{e}, \boldsymbol{f}' \rangle = a - a = 0$ and $\langle \boldsymbol{f}', \boldsymbol{g} \rangle + \langle \boldsymbol{f}, \boldsymbol{g}' \rangle = b - b = 0$. The Euclidean-type system $\boldsymbol{f}' = -a\, \boldsymbol{e} + b\, \boldsymbol{g}$ gives $\langle \boldsymbol{e}', \boldsymbol{f} \rangle + \langle \boldsymbol{e}, \boldsymbol{f}' \rangle = 2a$, so it does not describe an orthonormal frame unless $a \equiv 0$.

Corollary 1. With $\boldsymbol{f} = \boldsymbol{n}$ and $\boldsymbol{g} = \boldsymbol{t} \wedge \boldsymbol{n}$, system (6) coincides with (3), so $a = \kappa$, $b = \tau$, $\boldsymbol{D} = \tau \boldsymbol{t} + \kappa\, \boldsymbol{t} \wedge \boldsymbol{n}$ and $\langle \boldsymbol{D}, \boldsymbol{D} \rangle = \kappa^2 - \tau^2$. In general $\kappa = |a|$ and $|\tau| = |b|$. In case (a), $\kappa = |\omega|\cosh\theta$ and $|\tau| = |\omega\sinh\theta|$, so $\kappa > |\tau|$. In case (b), $\kappa = |\omega\sinh\theta|$ and $|\tau| = |\omega|\cosh\theta$, so $\kappa < |\tau|$.

Remark 1. The hyperbolic parametrization of Proposition 1 is local, but the form (6)–(7) is global. A direct computation with (2) gives $\boldsymbol{D} \wedge \boldsymbol{e} = a\boldsymbol{f}$, $\boldsymbol{D} \wedge \boldsymbol{f} = a\boldsymbol{e} + b\boldsymbol{g}$ and $\boldsymbol{D} \wedge \boldsymbol{g} = -b\boldsymbol{f}$ for $\boldsymbol{D} = b\boldsymbol{e} + a\boldsymbol{g}$ and arbitrary smooth functions a, b. Equation (6) therefore remains valid where a vanishes and where $\boldsymbol{D}$ becomes null ($a = \pm b$), although θ is undefined at null points.

For constant coefficients the frame has a closed form. We collect the frame vectors as the columns of the matrix $F = (\boldsymbol{e}\ \boldsymbol{f}\ \boldsymbol{g})$, so that (6) reads $F' = FM$ with

$$M = \begin{pmatrix} 0 & a & 0 \\ a & 0 & -b \\ 0 & b & 0 \end{pmatrix}.$$

Direct multiplication gives $M^3 = (a^2 - b^2)\, M$, so the exponential series of sM collapses to three terms.

Proposition 2 (Closed-form frame)**.** For constant a, b the ribbon frame is $F(s) = F(0)\exp(sM)$, where

(8)

$$\exp(sM) = \begin{cases} I + \dfrac{\sinh\varpi s}{\varpi} M + \dfrac{\cosh\varpi s - 1}{\varpi^2} M^2, & a^2 > b^2,\ \varpi = \sqrt{a^2 - b^2}, \\ I + \dfrac{\sin\varpi s}{\varpi} M + \dfrac{1 - \cos\varpi s}{\varpi^2} M^2, & a^2 < b^2,\ \varpi = \sqrt{b^2 - a^2}, \\ I + s\,M + \dfrac{s^2}{2} M^2, & a^2 = b^2. \end{cases} \tag{132}$$

Proof. From $M^3 = (a^2 - b^2)M$ we get $M^{2k+1} = (a^2 - b^2)^k M$ and $M^{2k+2} = (a^2 - b^2)^k M^2$ for $k \geq 0$. Summing the even and odd parts of the exponential series gives the hyperbolic, trigonometric and polynomial forms. □

The three cases of (8) are a boost, a rotation and a null rotation of the frame, for a space-like, time-like and null Darboux vector. At $s = 1.7$ formula (8) agrees with a numerical matrix exponential to 2.2×10^{-15}.

The frame equations can be tested numerically. We integrated (6) and its Euclidean-type counterpart with constant coefficients and recorded the largest deviation of the Gram matrix $\langle \boldsymbol{X}_i, \boldsymbol{X}_j \rangle$ from $\mathrm{diag}(-1,1,1)$ (Fig. 1). For $a = 0.8$ and $b = 1.2$ the Euclidean-type system reaches 0.929 at $s = 1$ and 1.34 at $s = 3$, and for $a = 1.2$, $b = 0.8$ it reaches 1.69 and 2.00; the initial growth rate of $\langle \boldsymbol{e}, \boldsymbol{f} \rangle$ is $1.600 = 2a$, as Lemma 2 predicts. System (6) keeps the Gram error below 2.1×10^{-13}.

The map in Fig. 1(b) shows that the failure is controlled by the curvature alone: the error grows with $|a|$, saturates near 2 and is almost independent of b, because the torsion acts only on the space-like pair $\{\boldsymbol{f}, \boldsymbol{g}\}$. It vanishes only on the geodesic line $a = 0$. A fourth-order Runge–Kutta integration of (6) converges at the observed order 4.01, with a frame error of 4.1×10^{-10} at $h = 0.0125$ (panel c). The test separates a modeling error of order one from a controlled discretization error.

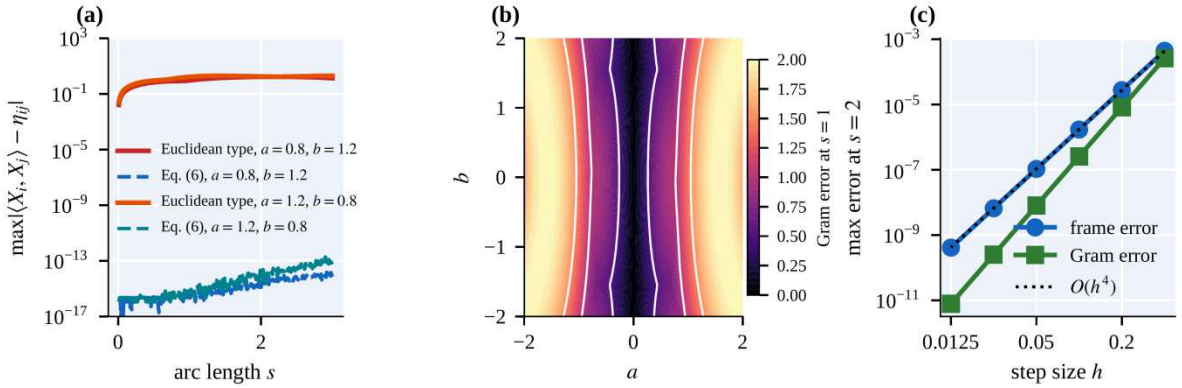


Fig. 1 Lorentzian ribbon equations versus the Euclidean-type transfer used in Ref. [20]. (a) Largest Gram-matrix error $\max|\langle \boldsymbol{X}_i, \boldsymbol{X}_j \rangle - \eta_{ij}|$, $\eta = \mathrm{diag}(-1,1,1)$, along exact solutions with constant a, b; the Euclidean-type system (solid) loses orthonormality at order one, Eq. (6) (dashed) stays at round-off. (b) Gram error of the Euclidean-type system at $s = 1$ over the (a, b) plane, with white contours at 0.5, 1 and 1.5; only the geodesic line $a = 0$ is error-free. (c) Convergence of a fourth-order Runge–Kutta integration of Eq. (6) for $a = 0.8$, $b = 1.2$ at $s = 2$; the dotted line is an $O(h^4)$ guide

The ribbon frame also contains the non-rotating frame of the observer. The next statement identifies it and gives the Lorentzian analogue of the Bishop angle.

Proposition 3 (Fermi–Walker frame)**.** Let $\boldsymbol{X}_1 = \cos\psi\, \boldsymbol{f} + \sin\psi\, \boldsymbol{g}$ and $\boldsymbol{X}_2 = \boldsymbol{e} \wedge \boldsymbol{X}_1 = -\sin\psi\, \boldsymbol{f} + \cos\psi\, \boldsymbol{g}$. The vectors $\boldsymbol{X}_1, \boldsymbol{X}_2$ are Fermi–Walker parallel along $\boldsymbol{\gamma}$ if and only if $\psi' = -b$. In that case

$$\boldsymbol{e}' = k_1 \boldsymbol{X}_1 + k_2 \boldsymbol{X}_2, \qquad \boldsymbol{X}_1{}' = k_1 \boldsymbol{e}, \qquad \boldsymbol{X}_2{}' = k_2 \boldsymbol{e}, \qquad k_1 = a\cos\psi, \quad k_2 = -a\sin\psi, \tag{9}$$

which are the parallel-frame equations of a time-like curve [11]. The frame $\{\boldsymbol{e}, \boldsymbol{X}_1, \boldsymbol{X}_2\}$ is transported by the field $\boldsymbol{V}_{\mathrm{FW}} = a\,\boldsymbol{g}$.

Proof. From (6), ${\boldsymbol{X}_1}' = a\cos\psi\,\boldsymbol{e} + (\psi' + b)\boldsymbol{X}_2$ and $\langle \boldsymbol{X}_1, \boldsymbol{e}' \rangle = a\cos\psi$. By (5), $D_{\mathrm{FW}}\boldsymbol{X}_1/ds = (\psi' + b)\boldsymbol{X}_2$, which vanishes if and only if $\psi' = -b$. The same computation gives $D_{\mathrm{FW}}\boldsymbol{X}_2/ds = -(\psi' + b)\boldsymbol{X}_1$. Equations (9) follow by substituting $\boldsymbol{f} = \cos\psi\,\boldsymbol{X}_1 - \sin\psi\,\boldsymbol{X}_2$. Finally, (2) gives $(a\boldsymbol{g}) \wedge \boldsymbol{e} = a\boldsymbol{f} = \boldsymbol{e}'$, $(a\boldsymbol{g}) \wedge \boldsymbol{X}_1 = a\cos\psi\,\boldsymbol{e} = {\boldsymbol{X}_1}'$ and $(a\boldsymbol{g}) \wedge \boldsymbol{X}_2 = -a\sin\psi\,\boldsymbol{e} = {\boldsymbol{X}_2}'$. □

Proposition 3 shows that the ribbon frame rotates relative to the gyroscope frame by the accumulated torsion $\int b\,ds$. This is the Lorentzian counterpart of the Euclidean relation between Frenet and Bishop frames, in which the Bishop angle is the integral of the torsion [9]. Section 8 shows that the same angle produces Thomas precession.

4 Magnetic curves with respect to the ribbon frame

Let $\boldsymbol{V}$ be a vector field along $\boldsymbol{\gamma}$ and let $\boldsymbol{\Phi}(\boldsymbol{X}) = \boldsymbol{V} \wedge \boldsymbol{X}$ be its Lorentz force. By (1), $\boldsymbol{\Phi}$ is skew-adjoint for the Lorentzian metric:

(10)

$$\langle \boldsymbol{\Phi}(\boldsymbol{X}), \boldsymbol{Y} \rangle + \langle \boldsymbol{X}, \boldsymbol{\Phi}(\boldsymbol{Y}) \rangle = 0.$$

Skew-adjointness is the property that makes $\boldsymbol{\Phi}$ the Lorentz force of an electromagnetic field, and it is the test that the Euclidean-type equations fail.

Definition 1. For $\boldsymbol{X} \in \{\boldsymbol{e}, \boldsymbol{f}, \boldsymbol{g}\}$, the curve $\boldsymbol{\gamma}$ is $\boldsymbol{X}$-magnetic if $\nabla_{\boldsymbol{\gamma}'}\boldsymbol{X} = \boldsymbol{\Phi}(\boldsymbol{X})$. For $\boldsymbol{X} = \boldsymbol{e} = \boldsymbol{\gamma}'$ this is the equation of a magnetic trajectory.

For $\boldsymbol{V} = x\,\boldsymbol{e} + y\,\boldsymbol{f} + z\,\boldsymbol{g}$, Lemma 1 gives

(11)

$$\boldsymbol{V} \wedge \boldsymbol{e} = z\,\boldsymbol{f} - y\,\boldsymbol{g}, \qquad \boldsymbol{V} \wedge \boldsymbol{f} = z\,\boldsymbol{e} + x\,\boldsymbol{g}, \qquad \boldsymbol{V} \wedge \boldsymbol{g} = -y\,\boldsymbol{e} - x\,\boldsymbol{f}.$$

Each characterization below follows by comparing (11) with (6).

Theorem 1 ($\boldsymbol{e}$-magnetic curves)**.** The curve $\boldsymbol{\gamma}$ is $\boldsymbol{e}$-magnetic if and only if, for some function Ω,

(12)

$$\boldsymbol{V} = \Omega\,\boldsymbol{e} + a\,\boldsymbol{g},$$

and then

(13)

$$\boldsymbol{\Phi}(\boldsymbol{e}) = a\,\boldsymbol{f}, \qquad \boldsymbol{\Phi}(\boldsymbol{f}) = a\,\boldsymbol{e} + \Omega\,\boldsymbol{g}, \qquad \boldsymbol{\Phi}(\boldsymbol{g}) = -\Omega\,\boldsymbol{f}.$$

Proof. The condition $\boldsymbol{\Phi}(\boldsymbol{e}) = \boldsymbol{e}' = a\boldsymbol{f}$ and (11) give $z\boldsymbol{f} - y\boldsymbol{g} = a\boldsymbol{f}$, so $y = 0$ and $z = a$, while $x =: \Omega$ is free. The converse and (13) follow from (11). □

Theorem 2 ($\boldsymbol{f}$-magnetic curves)**.** The curve $\boldsymbol{\gamma}$ is $\boldsymbol{f}$-magnetic if and only if, for some function λ,

(14)

$$\boldsymbol{V} = b\,\boldsymbol{e} - \lambda\,\boldsymbol{f} + a\,\boldsymbol{g},$$

and then

(15)

$$\boldsymbol{\Phi}(\boldsymbol{e}) = a\,\boldsymbol{f} + \lambda\,\boldsymbol{g}, \qquad \boldsymbol{\Phi}(\boldsymbol{f}) = a\,\boldsymbol{e} + b\,\boldsymbol{g}, \qquad \boldsymbol{\Phi}(\boldsymbol{g}) = \lambda\,\boldsymbol{e} - b\,\boldsymbol{f}.$$

Proof. The condition $\boldsymbol{\Phi}(\boldsymbol{f}) = \boldsymbol{f}' = a\boldsymbol{e} + b\boldsymbol{g}$ and (11) give $z = a$ and $x = b$, while $y =: -\lambda$ is free. The converse and (15) follow from (11). □

Theorem 3 ($\boldsymbol{g}$-magnetic curves)**.** The curve $\boldsymbol{\gamma}$ is $\boldsymbol{g}$-magnetic if and only if, for some function Ω_2,

$$\boldsymbol{V} = b\,\boldsymbol{e} + \Omega_2\,\boldsymbol{g}, \tag{16}$$

and then

$$\boldsymbol{\Phi}(\boldsymbol{e}) = \Omega_2\,\boldsymbol{f}, \qquad \boldsymbol{\Phi}(\boldsymbol{f}) = \Omega_2\,\boldsymbol{e} + b\,\boldsymbol{g}, \qquad \boldsymbol{\Phi}(\boldsymbol{g}) = -b\,\boldsymbol{f}. \tag{17}$$

Proof. The condition $\boldsymbol{\Phi}(\boldsymbol{g}) = \boldsymbol{g}' = -b\boldsymbol{f}$ and (11) give $y = 0$ and $x = b$, while $z =: \Omega_2$ is free. The converse and (17) follow from (11). □

An immediate consequence of Theorem 1 concerns the invariant of the field. Along an $\boldsymbol{e}$-magnetic curve,

$$\langle \boldsymbol{V}, \boldsymbol{V} \rangle = a^2 - \Omega^2, \tag{18}$$

so the squared signed curvature equals $\Omega^2 + \langle \boldsymbol{V}, \boldsymbol{V} \rangle$ at every point. Section 6 shows that this identity fixes the curvature by position for Killing fields. The three families intersect in a single field. The next theorem shows that this field is the Darboux vector, which is the Lorentzian analogue of the angular velocity of a rigid frame.

Theorem 4 (Larmor-type theorem)**.** The following statements are equivalent: (i) $\boldsymbol{e}' = \boldsymbol{V} \wedge \boldsymbol{e}$, $\boldsymbol{f}' = \boldsymbol{V} \wedge \boldsymbol{f}$ and $\boldsymbol{g}' = \boldsymbol{V} \wedge \boldsymbol{g}$; (ii) $\boldsymbol{V} = \boldsymbol{D} = b\,\boldsymbol{e} + a\,\boldsymbol{g}$; (iii) $\boldsymbol{\gamma}$ is $\boldsymbol{e}$-magnetic and $\boldsymbol{f}$-magnetic; (iv) $\boldsymbol{\gamma}$ is $\boldsymbol{e}$-magnetic and $\boldsymbol{g}$-magnetic.

Proof. (i)⇔(ii): by (4), $\boldsymbol{X}' = \boldsymbol{D} \wedge \boldsymbol{X}$, and if $\boldsymbol{V} \wedge \boldsymbol{X} = \boldsymbol{D} \wedge \boldsymbol{X}$ on a basis then $\boldsymbol{V} = \boldsymbol{D}$, because $\boldsymbol{X} \mapsto (\boldsymbol{V} - \boldsymbol{D}) \wedge \boldsymbol{X}$ vanishes only for $\boldsymbol{V} = \boldsymbol{D}$. For (iii), equating (12) and (14) gives $\Omega = b$ and $\lambda = 0$. For (iv), equating (12) and (16) gives $\Omega = b$ and $\Omega_2 = a$. The converses follow from Theorems 1–3. □

The ribbon frame differs from the Frenet frame at inflection points. In the Frenet approach $\kappa = |a| > 0$ is required, and $\boldsymbol{n}$ is discontinuous where a changes sign. In the ribbon frame a is a smooth signed curvature, and Theorems 1–4 hold on any interval, including zeros of a.

Example 1. Take $a(s) = s$ and $b \equiv 1$. On $|s| < 1$ the Darboux vector is time-like, with $\omega = \sqrt{1 - s^2}$ and $\tanh\theta = s$. At $s = \pm 1$ it is null, and for $|s| > 1$ it is space-like. By Remark 1, Eq. (6) holds on the whole line, and the field $\boldsymbol{V} = \Omega\boldsymbol{e} + s\,\boldsymbol{g}$ makes $\boldsymbol{\gamma}$ $\boldsymbol{e}$-magnetic for every Ω. The Frenet frame is undefined at $s = 0$.

We integrated Example 1 on $|s| \le 1.6$ with the Dormand–Prince method (tolerance 10^{-12}). Fig. 2(a,b) shows that $\boldsymbol{f}$ keeps its orientation through the apex, whereas the Frenet normal $\boldsymbol{n} = \operatorname{sgn}(a)\,\boldsymbol{f}$ reverses: across $s = 0$ (grid spacing 0.004) the components of $\boldsymbol{f}$ change by at most 0.008, while those of $\boldsymbol{n}$ jump by 2.000. The binormal flips as well, although the Frenet torsion stays equal to $b = 1$, because the two sign changes cancel.

Panel (c) gives the electromagnetic reading of Section 5 for $\boldsymbol{V} = \boldsymbol{D}$. The rest-frame electric field equals $a = s$ and changes sign at the inflection point, the magnetic field equals $b = 1$, and the invariant $a^2 - b^2$ changes sign at $|s| = 1$. Along the computed solution the frame stays orthonormal to 9.7×10^{-13}, and $\boldsymbol{X}' = \boldsymbol{D} \wedge \boldsymbol{X}$ holds to 5.3×10^{-13}, including the two null points. The ribbon frame can therefore follow a trajectory through a reversal of the transverse force.

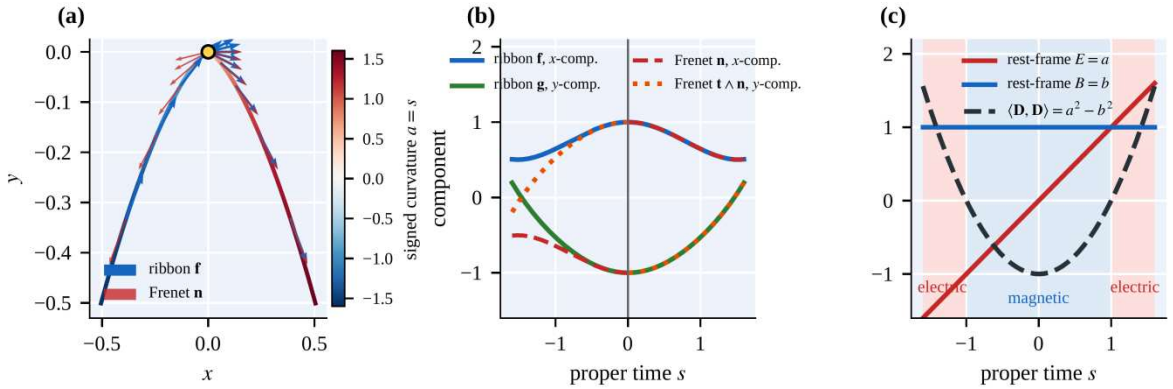


Fig. 2 Ribbon frame through an inflection point, Example 1 with $a(s) = s$, $b \equiv 1$. (a) Spatial projection of the worldline colored by the signed curvature, with the spatial parts of the ribbon vector $\boldsymbol{f}$ (blue) and the Frenet normal $\boldsymbol{n}$ (red); the dot marks $s = 0$. (b) Components of $\boldsymbol{f}$, $\boldsymbol{g}$, $\boldsymbol{n}$ and $\boldsymbol{t} \wedge \boldsymbol{n}$ against proper time; the Frenet vectors jump at $s = 0$ while the ribbon vectors stay smooth. (c) Rest-frame electric field a, magnetic field b and invariant $\langle \boldsymbol{D}, \boldsymbol{D} \rangle = a^2 - b^2$ for $\boldsymbol{V} = \boldsymbol{D}$; shading marks magnetic-dominated ($|s| < 1$) and electric-dominated ($|s| > 1$) parts

5 Electromagnetic reading in 2+1 dimensions

Consider a particle of mass m and charge q whose worldline $\boldsymbol{\gamma}$ is parametrized by proper time. The Lorentz law is $m\nabla_{\boldsymbol{\gamma}'}\boldsymbol{\gamma}' = q\boldsymbol{F}(\boldsymbol{\gamma}')$ with a skew-adjoint field tensor $\boldsymbol{F}$. In dimension three every skew-adjoint map has the form $\boldsymbol{F}(\boldsymbol{X}) = \boldsymbol{V} \wedge \boldsymbol{X}$, so $\boldsymbol{V}$ encodes the electric and magnetic fields of $(2+1)$-dimensional electrodynamics [37]. We take $q/m = 1$. Applying $\boldsymbol{\Phi}$ to the vectors of a moving frame follows the strategy of Ref. [18], and the signs in (13)–(17) are the ones required by (10).

For a laboratory observer with four-velocity $\partial_t = (0,0,1)$, the definitions below give $B = V_3$ and $\boldsymbol{E} = (-V_2, V_1, 0)$. A slow particle then obeys $\ddot{\boldsymbol{x}} = \boldsymbol{E} + \dot{\boldsymbol{x}} \times B\hat{\boldsymbol{z}}$, the planar Lorentz law with B along the normal of the plane. Relative to a general observer $\boldsymbol{e}$ we put

(19)

$$B := -\langle \boldsymbol{V}, \boldsymbol{e} \rangle, \qquad \boldsymbol{E} := \boldsymbol{V} \wedge \boldsymbol{e} \in \boldsymbol{e}^{\perp}.$$

Here B is the pseudo-scalar magnetic field and $\boldsymbol{E}$ the electric field in the rest frame of $\boldsymbol{e}$. The quantity

(20)

$$\langle \boldsymbol{V}, \boldsymbol{V} \rangle = |\boldsymbol{E}|^2 - B^2$$

is invariant. A negative value means a magnetic-dominated field, for which some observer sees $\boldsymbol{E} = \boldsymbol{0}$. A positive value means an electric-dominated field, for which some observer sees $B = 0$. For $\boldsymbol{V} = x\boldsymbol{e} + y\boldsymbol{f} + z\boldsymbol{g}$, Eq. (11) gives $B = x$ and $\boldsymbol{E} = z\boldsymbol{f} - y\boldsymbol{g}$, which yields Table 2.

Table 2 Rest-frame magnetic and electric fields along the magnetic curves of Theorems 1–4, from Eq. (19)

	Rest-frame B	Rest-frame $\boldsymbol{E}$
$\boldsymbol{e}$-magnetic	Ω (free)	$a\boldsymbol{f}$
$\boldsymbol{f}$-magnetic	b	$a\boldsymbol{f} + \lambda\boldsymbol{g}$
$\boldsymbol{g}$-magnetic	b	$\Omega_2\boldsymbol{f}$
$\boldsymbol{V} = \boldsymbol{D}$ (Theorem 4)	b	$a\boldsymbol{f}$
$\boldsymbol{V} = \boldsymbol{V}_{\mathrm{FW}}$ (Proposition 3)	0	$a\boldsymbol{f}$

Corollary 2. For the field $\boldsymbol{V} = \boldsymbol{D}$ that transports the whole frame, with $\boldsymbol{f} = \boldsymbol{n}$, the rest-frame electric field has magnitude κ and the rest-frame magnetic field equals τ. Curvature is therefore an electric field and torsion a magnetic field in the instantaneous rest frame, and $\langle \boldsymbol{D}, \boldsymbol{D} \rangle = \kappa^2 - \tau^2$. Case (a) of Proposition 1 is electric-dominated and case (b) is magnetic-dominated.

Table 2 gives each free function a physical meaning. For an $\boldsymbol{e}$-magnetic curve the electric field is fixed, because it must supply the proper acceleration $a\boldsymbol{f}$, whereas the magnetic field Ω is free, because it exerts no force on a particle at rest. Section 8 shows that Ω controls the rotation of the spin. Theorem 4 is a relativistic analogue of Larmor precession: the frame rotates about a time-like $\boldsymbol{D}$ and is boosted about a space-like $\boldsymbol{D}$.

6 Killing magnetic fields

A magnetic field on $\mathbb{E}_1^3$ is a divergence-free vector field, and the standard choice is a Killing field [5]. Killing fields generate isometries, so they model fields with a continuous symmetry, such as a uniform magnetic field combined with a radial electric field.

Lemma 3. The Killing fields of $\mathbb{E}_1^3$ are exactly $\boldsymbol{K}(\boldsymbol{p}) = \boldsymbol{u} + \boldsymbol{w} \wedge \boldsymbol{p}$ with constant $\boldsymbol{u}, \boldsymbol{w} \in \mathbb{E}_1^3$. They are divergence-free, $\frac{d}{ds}\boldsymbol{K}\big(\boldsymbol{\gamma}(s)\big) = \boldsymbol{w} \wedge \boldsymbol{\gamma}'(s)$ along any curve, and $\langle \boldsymbol{w}, \boldsymbol{K} \rangle = \langle \boldsymbol{w}, \boldsymbol{u} \rangle$ everywhere.

Proof. The space $\mathbb{E}_1^3$ is flat, so its Killing fields are affine [38], $\boldsymbol{K}(\boldsymbol{p}) = \boldsymbol{u} + A\boldsymbol{p}$ with A skew-adjoint. The space of such A is three-dimensional, and $\boldsymbol{w} \mapsto \boldsymbol{w} \wedge (\cdot)$ is an injective linear map into it, hence onto. Then $\mathrm{tr}A = 0$ gives $\mathrm{div}\boldsymbol{K} = 0$. The last claim follows from (1). □

We write $\boldsymbol{w} = w_1\boldsymbol{e} + w_2\boldsymbol{f} + w_3\boldsymbol{g}$ with $w_1 = -\langle \boldsymbol{w}, \boldsymbol{e} \rangle$, $w_2 = \langle \boldsymbol{w}, \boldsymbol{f} \rangle$ and $w_3 = \langle \boldsymbol{w}, \boldsymbol{g} \rangle$.

Theorem 5. Let $\boldsymbol{\gamma}$ be a unit-speed time-like curve with ribbon frame (6) and let $\boldsymbol{K}(\boldsymbol{p}) = \boldsymbol{u} + \boldsymbol{w} \wedge \boldsymbol{p}$ be a Killing field. Then $\nabla_{\boldsymbol{\gamma}'}\boldsymbol{\gamma}' = \boldsymbol{K} \wedge \boldsymbol{\gamma}'$ if and only if there is a constant Ω such that

(21)

$$a' = -w_2, \qquad a\,(\Omega - b) = w_3,$$

and $\boldsymbol{K}\big(\boldsymbol{\gamma}(s_0)\big) = (\Omega\,\boldsymbol{e} + a\,\boldsymbol{g})(s_0)$ at one point s_0. In that case $\boldsymbol{K} \circ \boldsymbol{\gamma} = \Omega\,\boldsymbol{e} + a\,\boldsymbol{g}$ everywhere, $\Omega = -\langle \boldsymbol{K}, \boldsymbol{\gamma}' \rangle$ is a first integral, and

(22)

$$-w_1\,\Omega + a\,w_3 = \langle \boldsymbol{w}, \boldsymbol{u} \rangle = \mathrm{const.}$$

Proof. (⇒) Put $\boldsymbol{V} := \boldsymbol{K} \circ \boldsymbol{\gamma}$. Then $\boldsymbol{V} \wedge \boldsymbol{e} = \boldsymbol{e}'$, so by Theorem 1, $\boldsymbol{V} = \Omega\boldsymbol{e} + a\boldsymbol{g}$ with $\Omega = -\langle \boldsymbol{V}, \boldsymbol{e} \rangle$. By Lemma 3 and (11), $\boldsymbol{V}' = \boldsymbol{w} \wedge \boldsymbol{e} = w_3\boldsymbol{f} - w_2\boldsymbol{g}$. On the other hand, (6) gives

$$\boldsymbol{V}' = \Omega'\boldsymbol{e} + a(\Omega - b)\boldsymbol{f} + a'\boldsymbol{g}.$$

Comparing coefficients gives $\Omega' = 0$, $a(\Omega - b) = w_3$ and $a' = -w_2$. (⇐) Put $\boldsymbol{V} := \Omega\boldsymbol{e} + a\boldsymbol{g}$. The same computation gives $\boldsymbol{V}' = \boldsymbol{w} \wedge \boldsymbol{e}$, so $(\boldsymbol{V} - \boldsymbol{w} \wedge \boldsymbol{\gamma})' = \boldsymbol{0}$. At s_0 the hypothesis gives $\boldsymbol{V} = \boldsymbol{u} + \boldsymbol{w} \wedge \boldsymbol{\gamma}$, hence $\boldsymbol{V} = \boldsymbol{K} \circ \boldsymbol{\gamma}$ everywhere and $\boldsymbol{K} \wedge \boldsymbol{e} = a\boldsymbol{f} = \boldsymbol{e}'$. Finally, (22) is the identity $\langle \boldsymbol{w}, \boldsymbol{V} \rangle = \langle \boldsymbol{w}, \boldsymbol{u} \rangle$ of Lemma 3. □

Corollary 3. Along a magnetic trajectory of a Killing field, the curvature and the ribbon torsion are determined by position and by the constant Ω:

(23)

$$a^2 = \Omega^2 + \langle \boldsymbol{K}, \boldsymbol{K} \rangle|_{\boldsymbol{\gamma}(s)}, \qquad b = \Omega - \frac{w_3}{a} \quad (a \neq 0).$$

With $\boldsymbol{f} = \boldsymbol{n}$ the Frenet torsion is $\tau = \Omega - w_3/\kappa$, and $\kappa' = -w_2$.

Proof. The first identity is (18) with $\boldsymbol{V} = \boldsymbol{K} \circ \boldsymbol{\gamma}$, and the second is the second equation of (21). □

Remark 2 (Noether reading of Ω)**.** The constant Ω is the conserved charge of the isometry generated by $\boldsymbol{K}$ itself: $\frac{d}{ds}\langle \boldsymbol{K}, \boldsymbol{\gamma}' \rangle = \langle \boldsymbol{w} \wedge \boldsymbol{\gamma}', \boldsymbol{\gamma}' \rangle + \langle \boldsymbol{K}, \boldsymbol{K} \wedge \boldsymbol{\gamma}' \rangle = 0$, since both terms are determinants with a repeated vector. No potential term enters, because $\boldsymbol{\Phi}(\boldsymbol{K}) = \boldsymbol{K} \wedge \boldsymbol{K} = \boldsymbol{0}$.

Example 2. Take $\boldsymbol{u} = (0,0,B_0)$ with $B_0 = 0.6$, $\boldsymbol{w} = (0,0,c)$ with $c = 0.35$, $\boldsymbol{\gamma}(0) = (0.4,0,0)$ and $\boldsymbol{\gamma}'(0) = (0.5,0.6,z_0)$ with $z_0 = \sqrt{1 + 0.5^2 + 0.6^2}$. Then $\boldsymbol{K} = (cy, -cx, B_0)$, and in the laboratory frame this is a uniform magnetic field B_0 together with the radial electric field $\boldsymbol{E} = c\,\boldsymbol{x}$. Here $\langle \boldsymbol{K}, \boldsymbol{K} \rangle = c^2 r^2 - B_0^2$ with $r = |\boldsymbol{x}|$, so Corollary 3 predicts $\kappa^2 = \Omega^2 - B_0^2 + c^2 r^2$.

We integrated $\boldsymbol{\gamma}'' = \boldsymbol{K}(\boldsymbol{\gamma}) \wedge \boldsymbol{\gamma}'$ for Example 2 with the Dormand–Prince method (relative and absolute tolerance 10^{-12}) and evaluated a, a', b and Ω from analytic derivatives of the solution (Supplementary information). Fig. 3(a) shows the spatial projection of the trajectory, which spirals outward while its curvature increases. On $0 \le s \le 3$ the conserved charge is $\Omega = 0.845315$ with a spread of 2.7×10^{-12}. The relation $a' = -w_2$ holds to 7.0×10^{-12}, the relation $a(\Omega - b) = w_3$ to 2.5×10^{-12}, and the left side of (22) differs from $\langle \boldsymbol{w}, \boldsymbol{u} \rangle = -0.21$ by at most 1.2×10^{-12} (panel c).

The curvature grows from 0.612 to 2.983, so the trajectory is not a helix, and the position formula (23) reproduces it to 1.3×10^{-11} (panel b). The ribbon torsion varies only between 0.403 and 0.422, approaching Ω from below as a grows, in agreement with $b = \Omega - w_3/a$. The residuals scale with the integrator tolerance, reaching 1.6×10^{-5} at 10^{-6} and 8.4×10^{-10} at 10^{-10}, so the identities are properties of the flow rather than artifacts of the discretization.

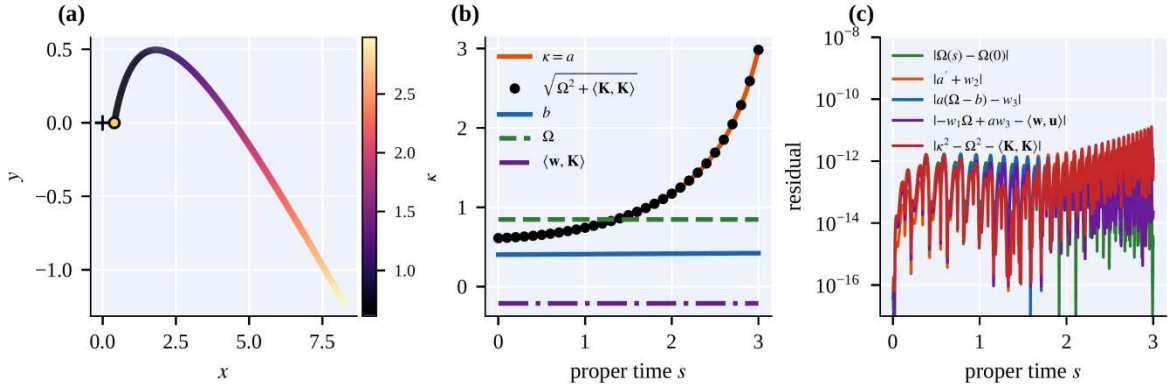


Fig. 3 Magnetic trajectory in the non-uniform Killing field of Example 2 ($B_0 = 0.6$, $c = 0.35$). (a) Spatial projection colored by the curvature κ; the dot marks the start and the cross the field axis. (b) Ribbon quantities along the trajectory: Ω and $\langle \boldsymbol{w}, \boldsymbol{K} \rangle$ are constant, $\kappa = a$ matches the position formula $\sqrt{\Omega^2 + \langle \boldsymbol{K}, \boldsymbol{K} \rangle}$ (dots) of Eq. (23), and b varies slowly. (c) Residuals of Theorem 5 and Corollary 3 on a logarithmic scale

The example also has time-translation and rotation symmetry, with charges $\mathcal{E} = \gamma_{\mathrm{L}} - cr^2/2$ and $\mathcal{L} = xy' - yx' + B_0 r^2/2$, where $\gamma_{\mathrm{L}} = t'$ is the laboratory Lorentz factor. Along the computed solution $\mathcal{E} = 1.240858$ and $\mathcal{L} = 0.288$ are conserved to 10^{-11}, and $\Omega = B_0\mathcal{E} + c\,\mathcal{L}$, because $\boldsymbol{K} = B_0\,\partial_t + c\,(y\,\partial_x - x\,\partial_y)$ combines the two generators.

Theorem 5 makes no assumption on the causal character of $\boldsymbol{w}$. We therefore repeated the computation with the same $\boldsymbol{u}$ and initial data for a space-like axis $\boldsymbol{w} = (0.35,0,0)$, which generates a boost, and a null axis $\boldsymbol{w} = (0.25,0,0.25)$, which generates a null rotation. The residuals in Table 3 are of the same size for all three types. For the space-like axis $\langle \boldsymbol{w}, \boldsymbol{u} \rangle = 0$, and the first integral (22) holds to 9.8×10^{-15}. The ribbon torsion varies more strongly, between 0.418 and 1.806 for the space-like axis and between 0.431 and 1.104 for the null axis, because w_3 changes sign along these trajectories.

Table 3 Largest residuals of Theorem 5 and Corollary 3 along computed trajectories. Three causal types of $\boldsymbol{w}$ at tolerance 10^{-12}

Case	Ω	spreadΩ	$\lvert a' + w_2 \rvert$	$\lvert a(\Omega - b) - w_3 \rvert$	Eq. (22)	Eq. (23)
time-like $\boldsymbol{w}$	0.845315	2.7×10^{-12}	7.0×10^{-12}	2.5×10^{-12}	1.2×10^{-12}	1.3×10^{-11}
space-like $\boldsymbol{w}$	0.761315	1.6×10^{-12}	4.0×10^{-12}	1.3×10^{-12}	9.8×10^{-15}	8.2×10^{-12}
null $\boldsymbol{w}$	0.821315	2.2×10^{-12}	4.5×10^{-12}	1.5×10^{-12}	8.0×10^{-13}	8.2×10^{-12}

All three solutions stop at a finite proper time, near $s = 3.67$, 5.07 and 6.32, respectively. For the time-like axis the two charges $\mathcal{E}$ and $\mathcal{L}$ reduce the problem to one radial equation, which explains this behavior exactly.

Proposition 4 (Radial reduction and escape time)**.** Along every magnetic trajectory of the field $\boldsymbol{K} = (cy, -cx, B_0)$, the radius $r(s)$ satisfies

$$r'' = \frac{c^2}{2}\, r^3 + \left(c\,\mathcal{E} - \frac{B_0^2}{4} \right) r + \frac{\mathcal{L}^2}{r^3}. \tag{24}$$

Hence $1/2\, r'^2 - U(r)$ is constant, with $U(r) = c^2/8\, r^4 + 1/2\, (c\mathcal{E} - B_0^2/4) r^2 - \mathcal{L}^2/(2r^2)$. If $c \neq 0$, $r'(0) > 0$ and r'^2 stays positive, the trajectory reaches $r = \infty$ at the finite proper time

$$s_* = \int_{r(0)}^{\infty} \frac{dr}{\sqrt{r'(0)^2 + 2\left[U(r) - U\big(r(0)\big)\right]}}. \tag{25}$$

Proof. In polar coordinates (r, ϕ) the spatial components of $\boldsymbol{\gamma}'' = \boldsymbol{K} \wedge \boldsymbol{\gamma}'$ give $r'' - r\phi'^2 = c\, r\, \gamma_{\mathrm{L}} + B_0\, r\phi'$ and $(r^2\phi')' = -B_0 r r'$. The second equation is the conservation of $\mathcal{L} = r^2\phi' + B_0 r^2/2$, and the time component gives ${\gamma_{\mathrm{L}}}' = c\, r r'$, which is the conservation of $\mathcal{E} = \gamma_{\mathrm{L}} - c r^2/2$. Substituting $\phi' = (\mathcal{L} - B_0 r^2/2)/r^2$ and $\gamma_{\mathrm{L}} = \mathcal{E} + c r^2/2$ into the radial equation gives (24) after cancellation of the terms in $B_0 \mathcal{L}/r$. Multiplying by r' and integrating gives the energy-like integral. Since $U(r) \sim c^2 r^4/8$, the integrand of (25) decays like $2/(c\, r^2)$, so the integral converges. □

For large r the cubic term of (24) dominates, and $r'' \simeq c^2 r^3/2$ has the blow-up solution

$$r \simeq \frac{2}{c\,(s_* - s)}, \qquad \gamma_{\mathrm{L}} \simeq \frac{2}{c\,(s_* - s)^2}, \qquad \kappa \simeq c\, r, \tag{26}$$

where the last relation follows from (23). Coordinate time $t = \int \gamma_{\mathrm{L}}\, ds$ then diverges like $(s_* - s)^{-1}$. The particle reaches spatial infinity only at infinite laboratory time, but it does so in finite proper time, because its speed approaches that of light. For Example 2 the coefficients of (24) are $c\mathcal{E} - B_0^2/4 = 0.3443$ and $\mathcal{L}^2 = 0.082944$,

with $r(0) = 0.4$ and $r'(0) = 0.5$. The radicand of (25) never falls below its initial value 0.25, and adaptive quadrature gives $s_* = 3.666761396$. Along the computed trajectory, Eq. (24) holds to a relative error of 8×10^{-8}, the accuracy of the finite-difference second derivative used for the check.

Fig. 4 tests these predictions. A linear fit of $1/r$ against s for $r > 10^3$ gives $s_* = 3.666761394$, within 2×10^{-9} of the quadrature (25), and a prefactor of 5.714276, compared with $2/c = 5.714286$. Log–log fits on $30 < r < 10^6$ give exponents -1.0005 for r, -0.993 for t, -1.0001 for κ and -1.999 for γ_{L}, in agreement with (26), and $1 - |\boldsymbol{v}|$ falls to 10^{-27} while t grows to 10^7. In a device such escape signals a defocusing electric field, and a wall at radius r_{wall} is reached about $2/(c\, r_{\mathrm{wall}})$ before s_*.

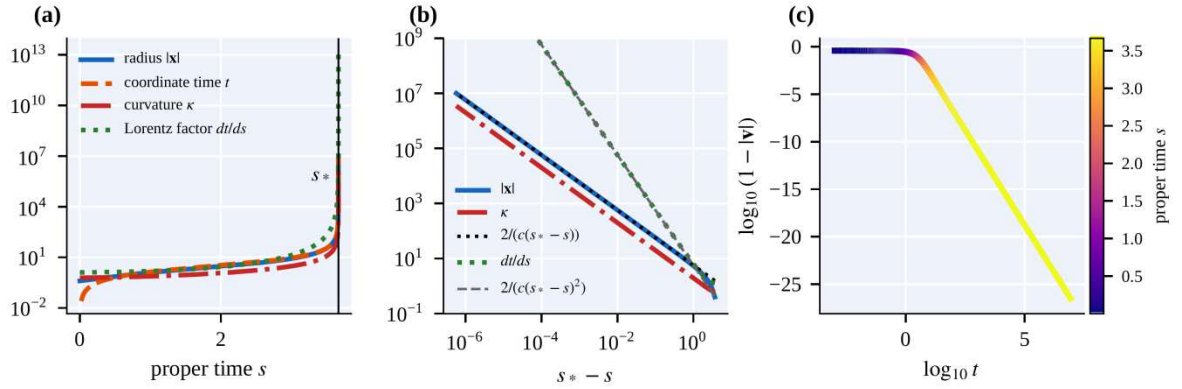


Fig. 4 Finite proper-time escape in the Killing field of Example 2. (a) Radius, coordinate time, curvature and Lorentz factor against proper time; the vertical line marks the extrapolated escape time $s_* = 3.666761$. (b) The same quantities against $s_* - s$ on logarithmic axes, with the asymptotic laws of Eq. (26) (dotted and dashed). (c) Approach to the speed of light, $\log_{10}(1 - |\boldsymbol{v}|)$ against $\log_{10} t$, colored by proper time

7 Uniform fields: cyclotron and hyperbolic motion

Uniform fields are the case $\boldsymbol{w} = \boldsymbol{0}$ of Theorem 5. They give the two textbook motions of relativistic mechanics, and the ribbon frame classifies them by the sign of a single invariant.

Theorem 6. Let $\boldsymbol{V}_0$ be a constant vector and let $\boldsymbol{\gamma}$ be $\boldsymbol{e}$-magnetic in $\boldsymbol{V}_0$ with $\kappa \neq 0$. Then κ and τ are constant, $\boldsymbol{V}_0 = \boldsymbol{D}$ and $\langle \boldsymbol{V}_0, \boldsymbol{V}_0 \rangle = \kappa^2 - \tau^2$. Conversely, a time-like curve with constant $\kappa \neq 0$ and τ is $\boldsymbol{e}$-magnetic in the constant field $\boldsymbol{D}$.

Proof. Theorem 5 with $\boldsymbol{w} = \boldsymbol{0}$ gives $a' = 0$ and $a(\Omega - b) = 0$, hence $\Omega = b$, and a, b are constant; then $\boldsymbol{V}_0 = \boldsymbol{D}$ by Theorem 4. Conversely, if a, b are constant, then $\boldsymbol{D}' = b\, a\boldsymbol{f} + a(-b\boldsymbol{f}) = \boldsymbol{0}$. □

Proposition 5. Up to Lorentz transformations, the curves of Theorem 6 are as follows. (a) Electric-dominated, $\kappa > |\tau|$, with $\varpi = \sqrt{\kappa^2 - \tau^2}$:

$$\boldsymbol{\gamma}(s) = (\kappa/\varpi^2\,(\cosh \varpi s - 1),\ -|\tau|/\varpi\ s,\ \kappa/\varpi^2 \sinh \varpi s).$$

(b) Magnetic-dominated, $\kappa < |\tau|$, with $\varpi = \sqrt{\tau^2 - \kappa^2}$:

$$\boldsymbol{\gamma}(s) = (\kappa/\varpi^2 \sin \varpi s,\ \kappa/\varpi^2\,(\cos \varpi s - 1),\ |\tau|/\varpi\ s).$$

Proof. (a) The tangent $\boldsymbol{\gamma}' = (\kappa/\varpi \sinh \varpi s, -|\tau|/\varpi, \kappa/\varpi \cosh \varpi s)$ has $\langle \boldsymbol{\gamma}', \boldsymbol{\gamma}' \rangle = -1$, and $\langle \boldsymbol{\gamma}'', \boldsymbol{\gamma}'' \rangle = \kappa^2$. With $\boldsymbol{f} = \boldsymbol{\gamma}''/\kappa$ and $\boldsymbol{g} = \boldsymbol{\gamma}' \wedge \boldsymbol{f}$ one finds $a = \kappa$, $b = -|\tau|$ (an orientation-dependent sign) and the constant

space-like vector $\boldsymbol{D} = (0, -\varpi, 0)$. (b) The tangent $\boldsymbol{\gamma}' = (\kappa/\varpi \cos\varpi s, -\kappa/\varpi \sin\varpi s, |\tau|/\varpi)$ has $\langle \boldsymbol{\gamma}', \boldsymbol{\gamma}' \rangle = -1$, and $\langle \boldsymbol{\gamma}'', \boldsymbol{\gamma}'' \rangle = \kappa^2$. The same construction gives $a = \kappa$, $b = |\tau|$ and the constant time-like vector $\boldsymbol{D} = (0,0,\varpi)$. □

In case (b) put $\kappa = |\omega| \sinh\theta$ and $|\tau| = |\omega| \cosh\theta$, so that $\varpi = |\omega|$. With $t = (|\tau|/\varpi)s$ the Lorentz factor and speed are $\gamma_{\mathrm{L}} = \cosh\theta$ and $v = \tanh\theta$, so θ is the rapidity. The spatial projection is a circle of radius $r = \kappa/\varpi^2 = \gamma_{\mathrm{L}} v/\varpi$, the relativistic Larmor radius $p/(qB_0)$, traversed at the cyclotron frequency $\varpi/\gamma_{\mathrm{L}}$, where $B_0 = \varpi$ is the field strength in the frame with $\boldsymbol{E} = \boldsymbol{0}$ [21].

In case (a) put $\kappa = |\omega| \cosh\theta$, $|\tau| = |\omega \sinh\theta|$ and $\varpi = |\omega|$. In the frame with $B = 0$ the field is purely electric, of strength ϖ, and the (x,t)-projection is the hyperbola $(x + \kappa/\varpi^2)^2 - t^2 = \kappa^2/\varpi^4$ [22], while the transverse momentum $p_y = -|\sinh\theta|$ is conserved. The boundary case $\kappa = |\tau|$ has a null $\boldsymbol{D}$ and is treated separately.

Proposition 6 (Null field)**.** Let a and b be constant with $a^2 = b^2 \neq 0$, so that $\boldsymbol{D} = b\boldsymbol{e} + a\boldsymbol{g}$ is null. Then

$$\boldsymbol{\gamma}(s) = \boldsymbol{\gamma}(0) + s\,\boldsymbol{e}_0 + \frac{s^2}{2}\,a\,\boldsymbol{f}_0 + \frac{s^3}{6}\,a\,(a\,\boldsymbol{e}_0 + b\,\boldsymbol{g}_0), \tag{27}$$

where $\boldsymbol{e}_0, \boldsymbol{f}_0, \boldsymbol{g}_0$ is the frame at $s = 0$.

Proof. By Proposition 2, $\boldsymbol{e}(s)$ is the first column of $F(0)(I + sM + s^2/2\,M^2)$. The first column of M is $(0, a, 0)^{\mathsf{T}}$ and that of M^2 is $(a^2, 0, ab)^{\mathsf{T}}$, so $\boldsymbol{e}(s) = \boldsymbol{e}_0 + s\,a\boldsymbol{f}_0 + s^2/2\,a(a\boldsymbol{e}_0 + b\boldsymbol{g}_0)$. Integrating once gives (27). □

The null worldline is a cubic polynomial in proper time. It describes motion in crossed electric and magnetic fields of equal strength, for which no observer sees a pure electric or a pure magnetic field. The cubic term points along the null vector $a\boldsymbol{e}_0 + b\boldsymbol{g}_0$, which is parallel to $\boldsymbol{D}$, so the particle is dragged towards the light-like direction of the field. For $a = b = 0.9$ an integration of (6) reproduces (27) to 5.3×10^{-15} on $0 \le s \le 3$, and the laboratory speed reaches 0.977 at $s = 3$.

The invariant $\kappa^2 - \tau^2$ thus separates the electric-dominated wedge $\kappa > |\tau|$ from the magnetic-dominated region, with the light-like lines $\kappa = \pm\tau$ as boundary. The helix with $\kappa = 1.15$ and $\tau = 1.74$ lies in the magnetic region and has Larmor radius 0.674, Lorentz factor 1.333 and speed 0.661; the example of case (a), with $\kappa = 1.75$ and $\tau = 1.15$, has $|p_y| = 0.872$. The Larmor radius diverges on approach to the null lines, where $\varpi \to 0$ and a particle sees almost equal electric and magnetic fields. The ratio $|\tau|/\varpi$ is the Lorentz factor in the magnetic region and the transverse momentum in the electric region, and it is constant along rays $\tau = \mu\kappa$, so the classification depends only on the ratio of rest-frame magnetic to electric field.

At fixed invariant strength ϖ, the cyclotron radius $\sinh\theta/\varpi$ grows with the rapidity while the laboratory angular frequency $\varpi/\cosh\theta$ decreases. This decrease of the revolution frequency with energy limits the classical cyclotron and led to the synchrocyclotron. For hyperbolic motion the vertex distance $\kappa/\varpi^2 = \cosh\theta/\varpi$ grows with the drift, because the conserved transverse momentum acts as an effective mass $\sqrt{1 + p_y^2}$ for the longitudinal motion.

With the Euclidean-type relations one would obtain $\boldsymbol{\Phi}(\boldsymbol{f}) = -a\boldsymbol{e} + \cdots$, for which $\langle \boldsymbol{\Phi}(\boldsymbol{e}), \boldsymbol{f} \rangle + \langle \boldsymbol{e}, \boldsymbol{\Phi}(\boldsymbol{f}) \rangle = 2a \neq 0$. Such a map is not skew-adjoint and is not the Lorentz force of any field. The signs in (13)–(17) are therefore forced by the Lorentz structure, and Fig. 1 quantifies the cost of ignoring them.

8 Spin transport in the ribbon frame

A particle with intrinsic angular momentum carries a spin vector $\boldsymbol{S}$, which is space-like, normalized and orthogonal to its four-velocity. When forces from field gradients are neglected, the spin obeys the BMT equation [21, 25]. We use its restriction to $(2+1)$ dimensions, which is the planar sector of the $(3+1)$-dimensional equation: the motion and the spin lie in the plane, B is normal to it and $\boldsymbol{E}$ lies in it.

Definition 2. Let $\boldsymbol{\gamma}$ be a magnetic trajectory of $\boldsymbol{V}$, so that $\boldsymbol{e}' = \boldsymbol{V} \wedge \boldsymbol{e}$. A spin field with gyromagnetic factor g is a field $\boldsymbol{S}$ along $\boldsymbol{\gamma}$ with $\langle \boldsymbol{S}, \boldsymbol{e} \rangle = 0$, $\langle \boldsymbol{S}, \boldsymbol{S} \rangle = 1$ and

(28)

$$\boldsymbol{S}' = \frac{g}{2}\, \boldsymbol{V} \wedge \boldsymbol{S} + \left(1 - \frac{g}{2}\right) \langle \boldsymbol{S}, \boldsymbol{e}' \rangle\, \boldsymbol{e}.$$

The anomaly is $\mathsf{a} = g/2 - 1$.

The second term of (28) is the unique correction along $\boldsymbol{e}$ that keeps $\boldsymbol{S}$ orthogonal to $\boldsymbol{e}$, since $\langle \boldsymbol{V} \wedge \boldsymbol{S}, \boldsymbol{e} \rangle = -\langle \boldsymbol{S}, \boldsymbol{e}' \rangle$ by (10), and the norm is preserved because $\langle \boldsymbol{S}, \boldsymbol{V} \wedge \boldsymbol{S} \rangle = 0$. For $g = 0$, Eq. (28) is Fermi–Walker transport (5); for $g = 2$ it is $\boldsymbol{S}' = \boldsymbol{V} \wedge \boldsymbol{S}$, the law of the velocity, so a Dirac particle has no anomalous precession.

Theorem 7 (Spin angle in the ribbon frame)**.** Let $\boldsymbol{\gamma}$ be $\boldsymbol{e}$-magnetic in $\boldsymbol{V}$, so that $\boldsymbol{V} = \Omega \boldsymbol{e} + a\boldsymbol{g}$ by Theorem 1, and write $\boldsymbol{S} = \cos\varphi\, \boldsymbol{f} + \sin\varphi\, \boldsymbol{g}$. Then $\boldsymbol{S}$ is a spin field with gyromagnetic factor g if and only if

(29)

$$\varphi' = \frac{g}{2}\, \Omega - b.$$

In words, the spin angle relative to the ribbon normal advances at $g/2$ times the rest-frame magnetic field minus the ribbon torsion.

Proof. By (2), $\boldsymbol{V} \wedge \boldsymbol{f} = \Omega \boldsymbol{g} + a\boldsymbol{e}$ and $\boldsymbol{V} \wedge \boldsymbol{g} = -\Omega \boldsymbol{f}$, and $\langle \boldsymbol{S}, \boldsymbol{e}' \rangle = a\cos\varphi$. The right side of (28) is therefore $a\cos\varphi\, \boldsymbol{e} + \frac{g}{2}\Omega(\cos\varphi\, \boldsymbol{g} - \sin\varphi\, \boldsymbol{f})$. By (6), the left side is $a\cos\varphi\, \boldsymbol{e} + (\varphi' + b)(\cos\varphi\, \boldsymbol{g} - \sin\varphi\, \boldsymbol{f})$. The two sides agree if and only if $\varphi' + b = \frac{g}{2}\Omega$. □

The angle equation (29) contains no curvature, so it holds through inflection points, and it holds in any field, uniform or not. Three special cases follow at once. For $g = 0$ it gives $\varphi' = -b$, which is Proposition 3: a gyroscope lags the ribbon frame by the accumulated torsion. For the frame-transporting field $\boldsymbol{V} = \boldsymbol{D}$ of Theorem 4 it gives $\varphi' = \mathsf{a}\, b$, so in a uniform field a particle with $g = 2$ keeps a fixed angle to the ribbon normal. For a Killing field Ω is constant, and integration gives

(30)

$$\varphi(s) = \varphi(0) + \frac{g}{2}\, \Omega\, s - \int_0^s b\; d\sigma.$$

Corollary 4 (Thomas precession and spin tune)**.** On the cyclotron orbit of Proposition 5(b) with Lorentz factor γ_{L}, the spin turns by $\mathsf{a}\gamma_{\mathrm{L}}$ revolutions per orbit relative to the momentum and by $1 + \mathsf{a}\gamma_{\mathrm{L}}$ revolutions per orbit relative to fixed laboratory axes. For $g = 0$ the laboratory rotation is $1 - \gamma_{\mathrm{L}}$ revolutions, the Thomas precession angle $2\pi(1 - \gamma_{\mathrm{L}})$ [24].

Proof. One orbit takes proper time $2\pi/\varpi$, and $|b| = |\tau| = \gamma_{\mathrm{L}}\varpi$ by Section 7. With $\Omega = b$, Eq. (29) gives $|\Delta\varphi| = |\mathsf{a}|\,|b|\, 2\pi/\varpi = 2\pi|\mathsf{a}|\gamma_{\mathrm{L}}$ per orbit. The vector $\boldsymbol{f}$ points towards the center, so the angle φ is measured

relative to the momentum direction, which itself turns once per orbit. The orientation conventions of Appendix A fix the sign, so that a positive anomaly makes the spin lead the momentum. □

We tested Theorem 7 by integrating (28) together with the trajectory. Along the Killing trajectory of Example 2, the computed angle agrees with (30) to 3.1×10^{-9} for $g = 0$, 2, 2.5 and 4 (Fig. 5a), an error set by the trapezoidal quadrature of $\int b\, ds$. The slope changes sign near $g = 2\bar{b}/\Omega \approx 0.98$, where $\bar{b}$ is the mean torsion and the magnetic torque balances the frame rotation.

Fig. 5(b) checks Corollary 4 in a uniform magnetic field. For $g = 0$, 1, 2 and 2.5 and Lorentz factors from 1.2 to 3, the measured rotation per orbit matches $1 + \mathrm{a}\gamma_\mathrm{L}$ to 2.1×10^{-10} revolutions. The Thomas line $1 - \gamma_\mathrm{L}$ is negative for every relativistic orbit, so a gyroscope rotates backwards in the laboratory, while $g = 2$ gives helicity locking at one revolution.

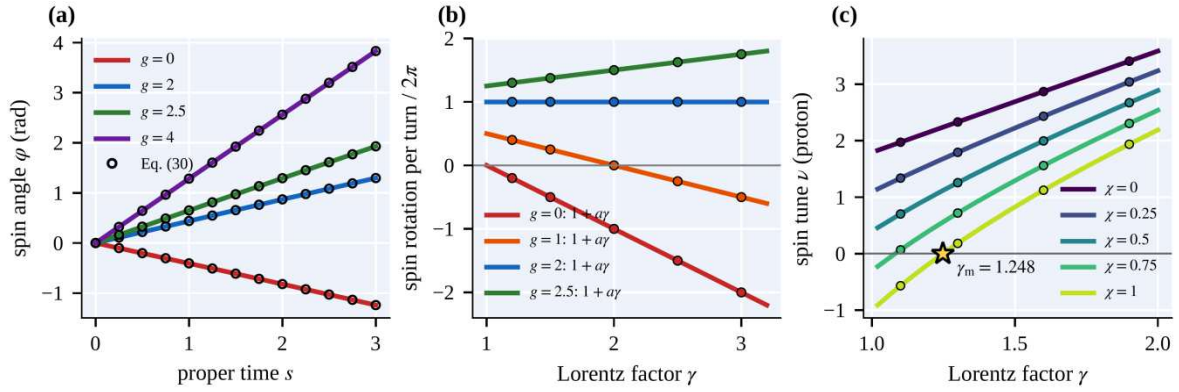


Fig. 5 Validation of the spin-angle equation (29). (a) Spin angle along the Killing trajectory of Example 2 for $g = 0$, 2, 2.5 and 4 (lines) compared with Eq. (30) (circles). (b) Spin rotation per orbit relative to laboratory axes in a uniform magnetic field: simulations (dots) and $1 + \mathrm{a}\gamma_\mathrm{L}$ (lines); $g = 0$ gives the Thomas result $1 - \gamma_\mathrm{L}$. (c) Spin tune ν of a proton ($\mathrm{a} = 1.79285$) on circular orbits with electric share χ of the centripetal force: simulations (dots) and Eq. (32) (lines); the star marks the magic Lorentz factor $\gamma_\mathrm{m} = 1.248$ of an all-electric ring

Storage rings combine a magnetic field with an electric field. The Killing field of Example 2 contains exactly this combination, a uniform B and a radial electric field $E_r = c\, r$, and it admits circular orbits centered on the axis. The next proposition evaluates Theorem 7 on these orbits.

Proposition 7 (Anomalous precession and spin tune)**.** Consider a counterclockwise circular orbit of radius R, speed v and Lorentz factor $\gamma = \gamma_\mathrm{L}$ in the field $\boldsymbol{K} = (cy, -cx, B)$, with $E_r = cR$ and $\gamma v^2/R = -(vB + E_r)$. Let $\omega_\mathrm{c} = v/R$ be the laboratory cyclotron frequency, $\omega_\mathrm{a} = \varphi'/\gamma$ the laboratory rate of the spin angle, and $\chi = E_r/(vB + E_r)$ the electric share of the centripetal force. Then

(31)

$$\omega_\mathrm{a} = \mathrm{a}B + \left(\mathrm{a} - \frac{1}{\gamma^2 - 1}\right) vE_r,$$

and the spin tune $\nu = -\omega_\mathrm{a}/\omega_\mathrm{c}$, the number of spin revolutions relative to the momentum per orbit, is

(32)

$$\nu = \mathrm{a}\gamma - \frac{\chi\,(1 + \mathrm{a})}{\gamma}.$$

Proof. Appendix A shows that $\kappa = \gamma^2 v^2/R$, $\Omega = \gamma(B + vE_r)$ and $w_3 = -c\gamma v$ on the orbit. Corollary 3 gives $b = \Omega - w_3/\kappa$, so (29) becomes $\varphi' = \mathrm{a}\,\Omega + w_3/\kappa = \mathrm{a}\gamma(B + vE_r) - E_r/(\gamma v)$. Dividing by γ and using

$\gamma^2 v^2 = \gamma^2 - 1$ gives (31). Substituting $E_r = -\chi\gamma v\,\omega_c$ and $B = -(1-\chi)\gamma\,\omega_c$, which follow from the orbit condition, gives (32) after simplification with $1 - v^2 = 1/\gamma^2$. □

Equation (31) is the planar form of the anomalous precession frequency on which the muon $g-2$ experiments rest [21, 26, 39]. Measuring ω_a and B determines the anomaly, which is then compared with Standard Model predictions [40, 41]. Three consequences are used in accelerator design. First, in a pure magnetic ring ($\chi = 0$) the spin tune is $\nu = a\gamma$. Second, at fixed B the electric term vanishes when $\gamma^2 = 1 + 1/a$, the magic Lorentz factor γ_m; at this energy electrostatic focusing does not disturb the measurement of a. Third, the spin is frozen to the momentum ($\nu = 0$) when

$$\chi_f = \frac{a\gamma^2}{1+a}, \tag{33}$$

and an all-electric ring ($\chi = 1$) is frozen exactly at γ_m. The magic momentum is $p_m = m\gamma_m v = m/\sqrt{a}$.

Fig. 5(c) tests (32) with the large proton anomaly, for which the electric term is visible. For χ from 0 to 1 and γ from 1.1 to 1.9, the simulated spin tune agrees with the formula to 4.4×10^{-11}. The all-electric curve crosses zero at $\gamma_m = 1.2481$. Table 4 evaluates the formulas for the electron, the muon, the proton and the deuteron with the CODATA 2018 constants [42] and the 2023 muon average [29]. The muon value $p_m = 3.0944\,\mathrm{GeV}/c$ is the operating momentum of the CERN, Brookhaven and Fermilab rings [26-28]. The proton value $0.70074\,\mathrm{GeV}/c$ is the design momentum of the proposed all-electric proton EDM ring [33, 34]. For the electron the magic momentum is only $15.006\,\mathrm{MeV}/c$, because its anomaly is close to that of the muon while its mass is 207 times smaller.

Table 4 Magic and frozen-spin parameters from Eqs. (32) and (33). Anomalies and masses from CODATA 2018 [42]; muon anomaly from the 2023 experimental average [29]. The last column gives the electric share needed to freeze the spin at $p = 1\,\mathrm{GeV}/c$

Particle	anomaly a	mass (GeV/c^2)	γ_m	p_m (GeV/c)	χ_f at 1 GeV/c
electron	1.15965×10^{-3}	5.10999×10^{-4}	29.38	0.015006	4.4×10^{3}
muon	1.16592×10^{-3}	0.105658	29.30	3.0944	0.1055
proton	1.79285	0.938272	1.2481	0.70074	1.371
deuteron	−0.142987	1.875613	–	–	−0.2143

Fig. 6 maps the spin tune over momentum and electric share. For the muon the frozen-spin curve rises from $\chi = 0$ at rest to $\chi = 1$ at the magic momentum, so below p_m a modest electric share suffices, which is the frozen-spin method for muon EDM searches [32]. For the proton the curve exceeds $\chi = 1$ above $0.7007\,\mathrm{GeV}/c$, where the magnetic force must point outward. For the deuteron the anomaly is negative, so freezing requires an electric force opposing the centripetal direction, 21% of the net force at $1\,\mathrm{GeV}/c$; deuteron EDM rings therefore combine electric and magnetic bending [32, 35].

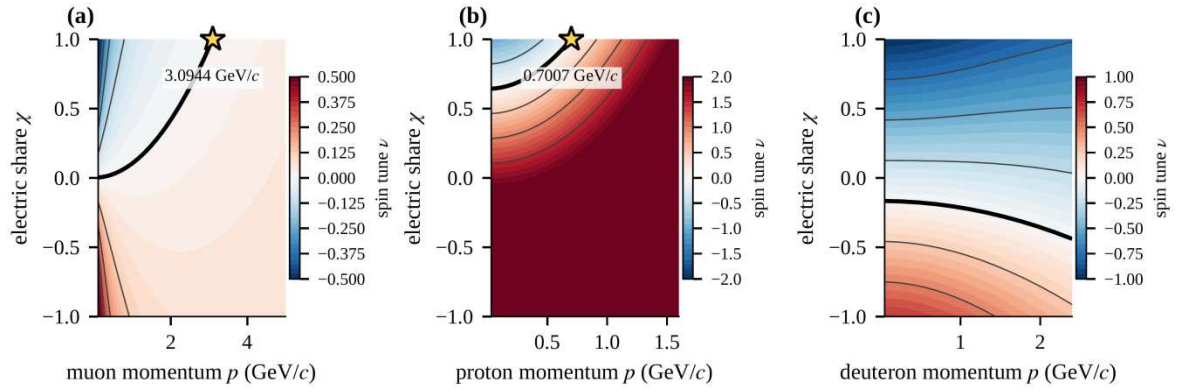


Fig. 6 Spin tune ν of Eq. (32) over momentum p and electric share χ of the centripetal force, with the frozen-spin curve $\nu = 0$ (thick black) and contours at fractions of the color range (thin). (a) Muon; the star marks the magic momentum $3.0944\,\mathrm{GeV}/c$. (b) Proton; magic momentum $0.7007\,\mathrm{GeV}/c$. (c) Deuteron with negative anomaly; the frozen-spin curve lies at $\chi < 0$

9 Discussion

The results form one chain. The Lorentzian signs of Lemma 1 fix the ribbon equations, which fix the field of every frame-adapted magnetic curve. The free function Ω is the rest-frame magnetic field; it is conserved in Killing fields, fixes the curvature by position and drives the spin angle. The torsion b enters both as the rest-frame magnetic field of the Darboux field and as the rotation of the ribbon frame relative to a gyroscope, and Thomas precession is the difference between these roles. Table 5 compares the results with previous studies. The ribbon-frame derivation does not improve on the BMT equation, which is exact in its domain; its value is a single scalar law that separates the field contribution $g\Omega/2$ from the geometric contribution $-b$.

Table 5 Comparison with previous studies. Numerical agreement refers to the computations of this paper

Quantity	Previous result	This work
Ribbon frame in $\mathbb{E}^3_1$	Euclidean signs transferred [20]	Lorentzian signs, Gram error $< 2.1 \times 10^{-13}$ versus order one
Killing magnetic curves	Frenet frame, $\kappa > 0$ [5]	signed curvature, $\kappa^2 = \Omega^2 + \langle \boldsymbol{K}, \boldsymbol{K} \rangle$, all causal types of $\boldsymbol{w}$
Frame-adapted magnetic curves	Frenet or Bishop frames [2, 3, 14, 18]	$\boldsymbol{e}$-, $\boldsymbol{f}$-, $\boldsymbol{g}$-magnetic curves with physical fields (Table 2)
Thomas precession per orbit	$2\pi(1-\gamma_\mathrm{L})$ [21, 24]	same from $\varphi' = -b$; error 2.1×10^{-10} rev
Spin tune, magnetic ring	$\mathrm{a}\gamma_\mathrm{L}$ [21, 39]	same from Eq. (29)
Muon magic momentum	$3.094\,\mathrm{GeV}/c$ [26]	$3.0944\,\mathrm{GeV}/c$, Eq. (32)
Proton magic momentum	$0.7007\,\mathrm{GeV}/c$ [33]	$0.70074\,\mathrm{GeV}/c$
Frozen-spin condition	combined E and B [32]	closed form $\chi_\mathrm{f} = \mathrm{a}\gamma^2/(1+\mathrm{a})$

The study has concrete limitations. We treat time-like curves only; space-like and null curves need separate ribbon parametrizations. The model is classical, without radiation reaction, back-reaction or Stern–Gerlach force. The $(2+1)$-dimensional setting covers in-plane spin in a normal magnetic field and an in-plane electric field; vertical spin, field gradients and electric dipole moments require the full BMT equation and a four-dimensional frame. The numerical tests verify identities and closed-form predictions and do not replace beam-dynamics codes with realistic field maps.

Three practical recommendations follow. The compatibility condition of Lemma 2 should be checked whenever a Euclidean frame is transferred to $\mathbb{E}_1^3$. The ribbon frame with signed curvature should replace the Frenet frame for trajectories through a reversal of the transverse force. In tracking with symmetric fields, Ω and Eq. (23) are inexpensive accuracy monitors, and Eqs. (32) and (33) give a closed-form starting point for ring design.

10 Conclusions

We derived the time-like ribbon frame of Minkowski 3-space with the Lorentzian cross product and developed its theory of magnetic curves, Killing fields and spin. The main findings are the following.

(1) The ribbon equations $\boldsymbol{e}' = a\boldsymbol{f}$, $\boldsymbol{f}' = a\boldsymbol{e} + b\boldsymbol{g}$, $\boldsymbol{g}' = -b\boldsymbol{f}$ preserve orthonormality; the Euclidean-type transfer produces a Gram error of order one.

(2) The $\boldsymbol{e}$-, $\boldsymbol{f}$- and $\boldsymbol{g}$-magnetic curves are characterized by explicit fields, the Darboux vector is the unique frame-transporting field, and the Fermi–Walker frame rotates relative to the ribbon frame by the accumulated torsion.

(3) For Killing fields, $a' = -w_2$ and $a(\Omega - b) = w_3$ hold with a conserved charge Ω, and $\kappa^2 = \Omega^2 + \langle \boldsymbol{K}, \boldsymbol{K} \rangle$; computed trajectories satisfy these identities to about 10^{-11} for all causal types of the axis.

(4) In a uniform magnetic and radial electric field the radius obeys an exact one-dimensional equation, and the escape time follows from a quadrature that agrees with the integration to 2×10^{-9}.

(5) Curvature and torsion are the rest-frame electric and magnetic fields; uniform fields give cyclotron, hyperbolic and, in the null case, cubic worldlines.

(6) The spin angle obeys $\varphi' = g\Omega/2 - b$, which reproduces Thomas precession, the spin tune $\mathsf{a}\gamma$, the magic momenta $3.0944\ \mathrm{GeV}/c$ (muon) and $0.70074\ \mathrm{GeV}/c$ (proton), and the frozen-spin condition.

Future work will extend the frame to space-like and null curves and to four-dimensional Minkowski space, where vertical spin motion and electric dipole moments enter.

Appendix A Orientation conventions and circular orbits

Consider the field $\boldsymbol{K} = (cy, -cx, B)$ and the point $(R, 0, t)$ of a counterclockwise circular orbit with speed v and Lorentz factor γ. Then $\boldsymbol{e} = \gamma(0, v, 1)$, the proper acceleration $\kappa = \gamma^2 v^2/R$ points to the center, $\boldsymbol{f} = (-1,0,0)$, and $\boldsymbol{g} = \boldsymbol{e} \wedge \boldsymbol{f} = (0, \gamma, \gamma v)$, whose spatial part points along the velocity. With $\boldsymbol{K} = (0, -cR, B)$ and $\boldsymbol{w} = (0,0,c)$ we obtain $\Omega = \gamma(B + vE_r)$ and $w_3 = -c\gamma v$, where $E_r = cR$. The x-component of $\boldsymbol{K} \wedge \boldsymbol{e}$, $\gamma(vB + E_r)$, must equal $-\kappa$, which is the orbit condition. In a pure magnetic field $B = -\gamma v/R < 0$ and $b = \Omega = \gamma B < 0$, so Eq. (29) gives $\varphi' = \mathsf{a}\gamma B < 0$ for $\mathsf{a} > 0$. Since φ increases from the inward normal towards the velocity, the spin then turns ahead of the momentum, and $\nu = -\omega_\mathrm{a}/\omega_\mathrm{c} = \mathsf{a}\gamma > 0$. For $g = 0$ the spin falls behind by γ revolutions per orbit, which leaves $1 - \gamma$ relative to fixed axes.

Supplementary information

Online Resource 1 contains the Python scripts (NumPy, SciPy) and their JSON diagnostics; every number in the text was copied from these files. Trajectories were integrated with the eighth-order Dormand–Prince method with dense output and tolerances of 10^{-6} to 10^{-13}, as stated with each result. Ribbon quantities were evaluated

without numerical differentiation from $\boldsymbol{e}'' = (\boldsymbol{w} \wedge \boldsymbol{e}) \wedge \boldsymbol{e} + \boldsymbol{K} \wedge \boldsymbol{e}'$, $a = \sqrt{\langle \boldsymbol{e}', \boldsymbol{e}' \rangle}$, $a' = \langle \boldsymbol{e}', \boldsymbol{e}'' \rangle / a$ and $b = \langle \boldsymbol{e}'', \boldsymbol{g} \rangle / a$. Spin angles were obtained as $\mathrm{atan2}(\langle \boldsymbol{S}, \boldsymbol{g} \rangle, \langle \boldsymbol{S}, \boldsymbol{f} \rangle)$ with phase unwrapping, and rates by least squares over two orbits. Running `ESM_1.py` reproduces the algebraic checks and Example 2 in a few seconds.

Statements and Declarations

Competing interests The authors have no relevant financial or non-financial interests to disclose.

Data availability The Python scripts and JSON diagnostics that produce every number, table and figure in this article are provided as Online Resource 1.

References

1. Barros M, Romero A (2007) Magnetic vortices. EPL 77:34002. https://doi.org/10.1209/0295-5075/77/34002
2. Bozkurt Z, Gök İ, Yaylı Y, Ekmekci FN (2014) A new approach for magnetic curves in 3D Riemannian manifolds. J Math Phys 55:053501. https://doi.org/10.1063/1.4870583
3. Özdemir Z, Gök İ, Yaylı Y, Ekmekci FN (2015) Notes on magnetic curves in 3D semi-Riemannian manifolds. Turk J Math 39:412–426. https://doi.org/10.3906/mat-1408-31
4. Chen B-Y, Aloui F, Khan MA, Choudhary MA (2025) Magnetic curves in differential geometry: a comprehensive survey. Mathematics 13:3849. https://doi.org/10.3390/math13233849
5. Druţă-Romaniuc SL, Munteanu MI (2013) Killing magnetic curves in a Minkowski 3-space. Nonlinear Anal Real World Appl 14:383–396. https://doi.org/10.1016/j.nonrwa.2012.07.002
6. Munteanu MI, Nistor AI (2012) The classification of Killing magnetic curves in $S^2 \times \mathbb{R}$. J Geom Phys 62:170–182. https://doi.org/10.1016/j.geomphys.2011.10.002
7. Jiang X, Pei D (2024) Geometric properties of lightlike magnetic curves and magnetic flux surfaces in Minkowski 3-space. Int J Geom Methods Mod Phys 21:2450119
8. Inoguchi J, Munteanu MI (2022) Magnetic Jacobi fields in 3-dimensional Sasakian space forms. J Geom Anal 32:96. https://doi.org/10.1007/s12220-021-00851-6
9. Bishop RL (1975) There is more than one way to frame a curve. Am Math Mon 82:246–251. https://doi.org/10.1080/00029890.1975.11993807
10. Farouki RT (2016) Rational rotation-minimizing frames—recent advances and open problems. Appl Math Comput 272:80–91. https://doi.org/10.1016/j.amc.2015.04.122
11. Özdemir M, Ergin AA (2008) Parallel frames of non-lightlike curves. Missouri J Math Sci 20:127–137. https://doi.org/10.35834/mjms/1316032813
12. Bohr J, Markvorsen S (2013) Ribbon crystals. PLoS ONE 8:e74932. https://doi.org/10.1371/journal.pone.0074932
13. Chirikjian GS (2013) Framed curves and knotted DNA. Biochem Soc Trans 41:635–638. https://doi.org/10.1042/BST20120346
14. Altınkaya A (2026) A unified approach to magnetic curves and flux surfaces via conjugate rotation minimizing frame. Proc Natl Acad Sci India Sect A Phys Sci. https://doi.org/10.1007/s40010-026-01185-0
15. Öztürk U, Öztürk EBK (2026) Non-helical loxodromes in the Heisenberg group. Proc Natl Acad Sci India Sect A Phys Sci. https://doi.org/10.1007/s40010-026-01242-8
16. Körpınar T, Demirkol RC (2018) Gravitational magnetic curves on 3D Riemannian manifolds. Int J Geom Methods Mod Phys 15:1850184. https://doi.org/10.1142/S0219887818501840
17. Körpınar T, Demirkol RC (2020) Electromagnetic curves of the linearly polarized light wave along an optical fiber in a 3D Riemannian manifold with Bishop equations. Optik 200:163334. https://doi.org/10.1016/j.ijleo.2019.163334
18. Körpınar T, Demirkol RC, Asil V, Körpınar Z (2022) Magnetic flux surfaces by the fractional Heisenberg antiferromagnetic flow of magnetic b-lines in binormal direction in Minkowski space. J Magn Magn Mater 549:168952. https://doi.org/10.1016/j.jmmm.2021.168952
19. Demirkol RC (2024) Pseudo-solitonic magnetic flows associated with nonlinear integrable systems in the Minkowski 3-space. Math Methods Appl Sci 47:4640–4659. https://doi.org/10.1002/mma.9831
20. Özdemir Y (2025) 3-Boyutlu Minkowski uzayda ribbon çatıya göre manyetik eğriler [Magnetic curves according to the ribbon frame in 3-dimensional Minkowski space] (in Turkish). Master's thesis, Fırat University, Elazığ
21. Jackson JD (1999) Classical electrodynamics, 3rd edn. Wiley, New York
22. Rindler W (2006) Relativity: special, general, and cosmological, 2nd edn. Oxford University Press, Oxford
23. Misner CW, Thorne KS, Wheeler JA (1973) Gravitation. W. H. Freeman, San Francisco
24. Thomas LH (1926) The motion of the spinning electron. Nature 117:514. https://doi.org/10.1038/117514a0

25. Bargmann V, Michel L, Telegdi VL (1959) Precession of the polarization of particles moving in a homogeneous electromagnetic field. Phys Rev Lett 2:435–436. https://doi.org/10.1103/PhysRevLett.2.435
26. Bailey J et al (1979) Final report on the CERN muon storage ring including the anomalous magnetic moment and the electric dipole moment of the muon, and a direct test of relativistic time dilation. Nucl Phys B 150:1–75. https://doi.org/10.1016/0550-3213(79)90292-X
27. Bennett GW et al (2006) Final report of the E821 muon anomalous magnetic moment measurement at BNL. Phys Rev D 73:072003. https://doi.org/10.1103/PhysRevD.73.072003
28. Abi B et al (2021) Measurement of the positive muon anomalous magnetic moment to 0.46 ppm. Phys Rev Lett 126:141801. https://doi.org/10.1103/PhysRevLett.126.141801
29. Aguillard DP et al (2023) Measurement of the positive muon anomalous magnetic moment to 0.20 ppm. Phys Rev Lett 131:161802. https://doi.org/10.1103/PhysRevLett.131.161802
30. Aguillard DP et al (2025) Measurement of the positive muon anomalous magnetic moment to 127 ppb. Phys Rev Lett 135:101802. https://doi.org/10.1103/7clf-sm2v
31. Abe M et al (2019) A new approach for measuring the muon anomalous magnetic moment and electric dipole moment. Prog Theor Exp Phys 2019:053C02. https://doi.org/10.1093/ptep/ptz030
32. Farley FJM et al (2004) New method of measuring electric dipole moments in storage rings. Phys Rev Lett 93:052001. https://doi.org/10.1103/PhysRevLett.93.052001
33. Abusaif F, Aggarwal A, Aksentev A et al (2021) Storage ring to search for electric dipole moments of charged particles: feasibility study. CERN Yellow Reports: Monographs, CERN-2021-003. CERN, Geneva. https://doi.org/10.23731/CYRM-2021-003
34. Alexander J et al (2022) The storage ring proton EDM experiment. arXiv:2205.00830. https://arxiv.org/abs/2205.00830
35. Karanth S, Stephenson EJ, Chang SP et al (2023) First search for axionlike particles in a storage ring using a polarized deuteron beam. Phys Rev X 13:031004. https://doi.org/10.1103/PhysRevX.13.031004
36. López R (2014) Differential geometry of curves and surfaces in Lorentz-Minkowski space. Int Electron J Geom 7:44–107. https://doi.org/10.36890/iejg.594497
37. Deser S, Jackiw R, Templeton S (1982) Topologically massive gauge theories. Ann Phys 140:372–411. https://doi.org/10.1016/0003-4916(82)90164-6
38. O'Neill B (1983) Semi-Riemannian geometry with applications to relativity. Academic Press, New York
39. Miller JP, de Rafael E, Roberts BL (2007) Muon (g−2): experiment and theory. Rep Prog Phys 70:795–881. https://doi.org/10.1088/0034-4885/70/5/R03
40. Borsanyi Sz et al (2021) Leading hadronic contribution to the muon magnetic moment from lattice QCD. Nature 593:51–55. https://doi.org/10.1038/s41586-021-03418-1
41. Aliberti R et al (2025) The anomalous magnetic moment of the muon in the Standard Model: an update. Phys Rep 1143:1–158. https://doi.org/10.1016/j.physrep.2025.08.002
42. Tiesinga E, Mohr PJ, Newell DB, Taylor BN (2021) CODATA recommended values of the fundamental physical constants: 2018. Rev Mod Phys 93:025010. https://doi.org/10.1103/RevModPhys.93.025010